

# Reliability Properties of Solderable Conductive Adhesives with Low-Melting-Point Alloy Fillers

Byung-Seung Yim<sup>1</sup>, Jeong Il Lee<sup>1</sup>, Yuseon Heo<sup>2</sup>, Jooheon Kim<sup>2</sup>,  
Seong Hyuk Lee<sup>1</sup>, Young-Eui Shin<sup>1</sup> and Jong-Min Kim<sup>1,\*</sup>

<sup>1</sup>School of Mechanical Engineering, Chung-Ang University, Seoul 156-756, Korea

<sup>2</sup>School of Chemical Engineering & Material Science, Chung-Ang University, Seoul 156-756, Korea

A solderable conductive adhesive (SCA) using low-melting-point alloy (LMPA) filler was developed to overcome the limitations of conventional electrically conductive adhesives (ECAs), which include their low electrical conductivity, increased contact resistance, and low joint strength. The SCA formed good metallurgical conduction path between the corresponding electrodes due to the rheology-coalescence-wetting behaviors of molten LMPA fillers in SCA. This study examined the reliability of SCA assembly through the thermal shock test (218 to 398 K, 1000 cycles) and the high temperature and high humidity test (358 K/85%RH, 1000 h). The electrical resistance of the SCA assembly with metallurgical interconnections was much more stable than those with conventional ICAs. Before the reliability tests, a scallop-type Cu<sub>6</sub>Sn<sub>5</sub> ( $\eta$ -phase) intermetallic compound (IMC) layer was formed on the Sn-plated Cu lead/LMPA and LMPA/Cu metallization interface based on the results of interfacial microstructure observations of quad flat packages (QFPs) that were assembled with SCA. After the reliability tests, the thickness of IMC layer increased with time, and Cu<sub>6</sub>Sn<sub>5</sub> ( $\eta$ -phase) and Cu<sub>3</sub>Sn ( $\epsilon$ -phase) were formed. In addition, the fracture surface exhibited a cleavage fracture mode with the fracture propagating along the Cu–Sn IMC/Sn–Bi interface. These results demonstrate that SCA assembly with metallurgical interconnection has stable electrical and mechanical bonding characteristics. [doi:10.2320/matertrans.MB201207]

(Received June 4, 2012; Accepted September 12, 2012; Published November 2, 2012)

**Keywords:** anisotropic conductive adhesive, coalescence, fluxing capability, intermetallic compounds, low-melting-point alloy, reliability, solderable conductive adhesive, wettability

## 1. Introduction

Electrically conductive adhesives (ECAs) consisting of a polymer resin and conductive fillers have been widely used in the field of microelectronic packaging due to their many advantages such as low temperature processing, fine pitch capability, simple processing, and compatibility with non-solderable materials.<sup>1,2)</sup>

There are two main types of ECAs: isotropic conductive adhesives (ICAs) and anisotropic conductive adhesives (ACAs). ICAs produce approximately equal electricity flow in all directions, while ACAs have a unidirectional electrical conductivity flow in the Z-axis through the conductive particles trapped between the corresponding electrodes. Due to the unidirectional conductivity and composition of ACAs, these adhesives have advantages such as flexibility and fine pitch capability. On the other hand, conventional ECAs form a conduction path through the physical/mechanical contact of conductive fillers during the curing process and, as a result, have several critical limitations such as low electrical conductivity, unstable contact resistance, and low impact and joint strength<sup>3,4)</sup> compared to metallurgical interconnections created using a conventional soldering technique. In order to improve their electrical and mechanical properties and their reliability, we developed functionalized SCAs with low-melting-point alloy (LMPA) fillers and an interconnection process. Stable electrical resistance<sup>5,6)</sup> and high bonding strength can be achieved by metallurgical interconnection of molten LMPA fillers in the polymer matrix.<sup>7,8)</sup>

In this study, the reliability of quad flat package (QFP) assembly using SCA was compared with those with conventional ICAs. In addition, we assessed the interfacial microstructure and fracture surface between the QFP lead and

substrate metallization through cross-sectional investigation and failure analysis.

## 2. Experimental

### 2.1 Materials

The SCA used in this study was mainly composed of a polymer matrix and LMPA filler particles. Diglycidyl ether of bisphenol F (DGEBA: Kukdo Chemical) epoxy resin, which is a base material of the polymer matrix, was used as the binder. 4-4'-diaminodiphenylmethane (DDM: TCI Korea Co.) and boron trifluoride-mono-ethylene amine (BF<sub>3</sub>MEA: Wako Pure Chemical) were used as a curing agent and catalyst, respectively. Carboxylic acid (Aldrich Chem. Co.) was used as a reductant to remove the oxide layer from the surfaces of the LMPA fillers and the electrode pad. The distributed LMPA filler material was Sn–58Bi (diameter: 45  $\mu$ m; Senju Metal Co.). As shown in the Fig. 1, the filler particles were uniformly distributed in the polymer matrix at 20 vol%. Sn–58Bi eutectic solder has a relatively low melting temperature of 412.15 K, higher ultimate tensile and shear strengths than those of the Sn–Pb eutectic solder and reliable wetting capability on various substrates.<sup>9)</sup> The compositions of the SCAs are shown in Table 1. Three kinds of conventional ICAs with Ag flakes (ICA 1, ICA 2 and ICA 3) were used in the comparison of reliability properties. The compositions and curing conditions of conventional ICAs are shown in Table 2.

A quad flat package (QFP: Topline) was used for the SCA interconnection process. The QFP had dimensions of 14  $\times$  14  $\times$  2.7 mm<sup>3</sup> and had a Sn-plated 44-pin I/O with a 1.0 mm lead pitch. The area of the printed circuit board (PCB) was 32  $\times$  32  $\times$  1.0 mm<sup>3</sup> with an 18  $\mu$ m-thick Cu-plated electrode. To examine the electrical properties, a daisy-chain pattern was formed in the QFP and PCB.

\*Corresponding author, E-mail: 0326kj@cau.ac.kr

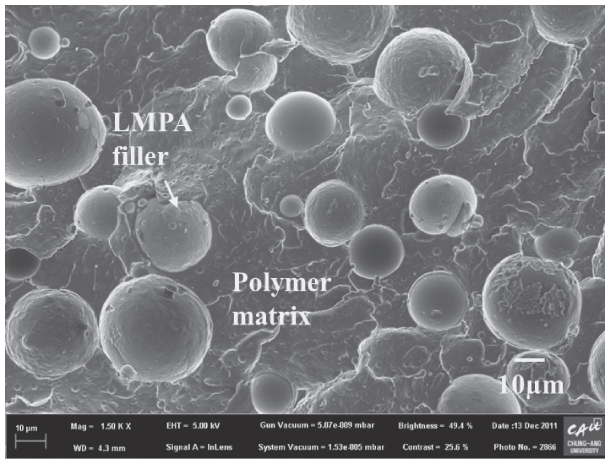


Fig. 1 Morphology of formulated SCAs with a polymer matrix and LMPA fillers.

Table 1 Composition of the SCAs used in this study.

Components	
Epoxy	DGEBF
Curing Agent	DDM
Catalyst	BF <sub>3</sub> MEA
Reductant	Carboxylic acid
LMPA Filler	Sn-58Bi ( $\phi$ 45 $\mu$ m, 20 vol%)

Table 2 Composition and curing condition of conventional ICAs.

	Polymer	Conductive Filler	Curing Condition
ICA 1	Epoxy-type		423 K, 30 min
ICA 2	Polyester-type	Ag-flake	393 K, 10 min
ICA 3	Epoxy-type		413 K, 40 min

## 2.2 Test method

### 2.2.1 SCA interconnection

To form the SCA interconnections, the substrate test board was sonicated for 1 min in acetone, rinsed with de-ionized water, and dried using an air-jet. A metal mask was aligned on the cleaned PCB board. Then, using the squeegee method, the formulated SCA was uniformly applied on the exposed whole electrodes of the PCB board at a thickness of 100  $\mu$ m. After the SCA was applied, the QFP test chip was aligned and mounted onto the corresponding electrode patterns using a flip chip bonder (LAMBDA: FINETECH Co.). Finally, the test vehicle was reflowed according to the temperature profile.

The temperature profile of the SCA interconnection consists of the solder reaction region and the polymer curing region. The solder reaction region was maintained at 433 K for 20 s, which was 20 K higher than melting point of LMPA filler. This created a conduction path between the electrodes due to the superior melting-rheology-wetting-coalescence behaviors of LMPA fillers. In addition, the polymer-curing region was maintained at 453 K for 80 s to obtain complete curing of the polymer matrix. Conduction paths were fixed by the contraction of the polymer matrix and SCA interconnection was completed.

Table 3 Reliability test conditions.

Test	Condition	Duration
Thermal shock test	218 to 398 K 30/30 min	1000 cycles
High temperature and high humidity test	358 K/85%RH	1000 h

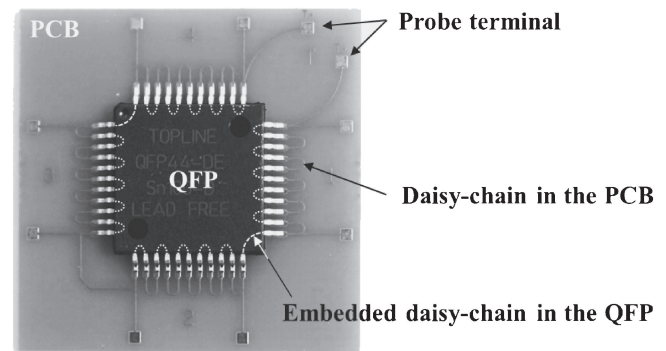


Fig. 2 Configuration of daisy-chain structure for electrical resistance test.

### 2.2.2 Reliability test

To examine the reliability properties of the SCA assembly, a thermal shock test and an aging test under high temperature and high humidity were performed.

The thermal shock test was performed using the JESD22-A106B C condition (218 to 398 K, 1000 cycles) using a thermal shock chamber (TSE-11-A: Espec Corp.) for monitoring the electrical resistance shift of the SCA assembly. The dwell time at each peak temperature was 30 min and the transition time between low and high temperatures was 10 s. The ramping and cooling rate of these cycles was approximately 18 K/s.

The high temperature and high humidity test was conducted using the JESD22-A101C condition (358 K/85%RH, 1000 h) using a constant temperature and humidity chamber (EN-GLMP-52: ENEX Co.) for monitoring the electrical resistance shift of the SCA assembly. The reliability test conditions are shown in Table 3.

All cured samples were tested using a multimeter (2750: Keithley Co.) to monitor to changes in total electrical resistance through the series circuit-type daisy-chain during the each reliability tests. The daisy-chain structure on the PCB and QFP test chip was shown in the Fig. 2. In addition, a 45-degree pull test was performed using a pull tester (PTR-1000, Rhesca Co.), with pull speed of 6 mm/min, in order to evaluate the mechanical integrity of the QFP joints. The pull strength of the QFP joints (22 leads) was measured before and after the reliability tests.

### 2.2.3 Cross-sectional investigation and failure analysis

To investigate the interface microstructure and fracture mode of SCAs before and after reliability tests, cross-sectional studies and failure analysis were conducted.

For the cross-sectional investigation, test specimens were molded on epoxy, then cross-sectioned using the polishing process. The microstructure of the bonding interface was examined by field-emission scanning electron microscopy

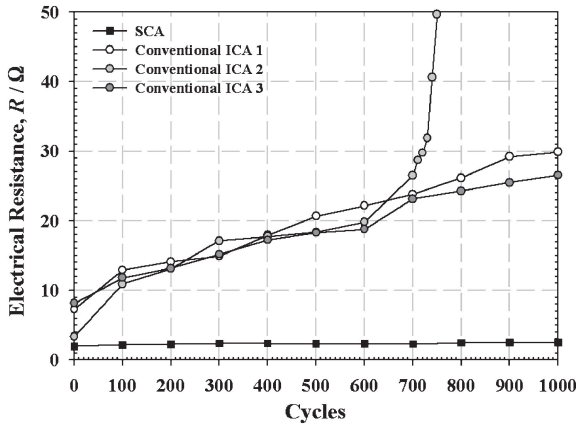


Fig. 3 The electrical resistance shift of conventional ICA and SCA assemblies during thermal shock test.

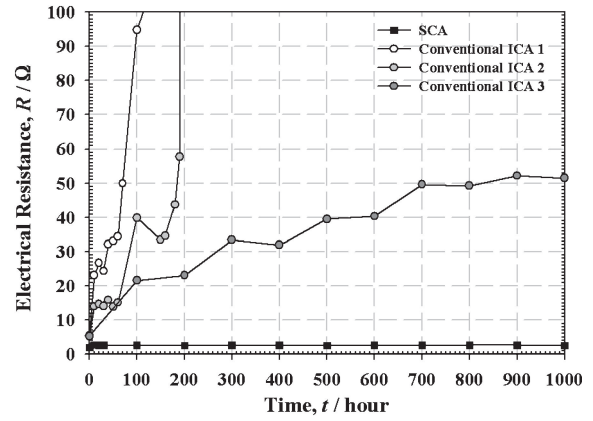


Fig. 4 The electrical resistance shift of conventional ICA and SCA assemblies during high temperature and high humidity test.

(FE-SEM: Sigma, Carl Zeiss Co. Ltd.) using back-scattered electron (BSE) mode. In addition, an energy dispersive spectrometer (EDS: NORAN System 7, Thermo Scientific) was used for chemical composition analysis of the inter-metallic compounds (IMCs).

In addition, the fracture mode of the joints was analyzed by assessing the morphology of the fracture surfaces and by chemical composition analysis of the fracture interfaces of the SCA joints after the 45-degree pull test.

### 3. Results and Discussion

#### 3.1 Reliability properties

To investigate the reliability properties of SCA assemblies, the thermal shock (218 to 398 K, 1000 cycles) and high temperature and high humidity (358 K/85%RH, 1000 h) tests were performed.

The electrical resistance shifts of conventional ICA and SCA assemblies during each reliability test are shown in Fig. 3 and Fig. 4, respectively. As can be seen the results, the initial electrical resistance of SCA assembly were lower than those of conventional ICA assemblies. Previous study in our laboratory has shown that reducing capability of SCA is essential for establishing proper wetting and coalescence behavior between metallizations and stable metallurgical interconnections.<sup>10)</sup> As such, we expected that the surface oxide films of particles and metallization to be almost or completely eliminated by the use of carboxylic acid reductant in formulated SCA.

As shown in Fig. 3, the electrical resistance of conventional ICA 1 and ICA 3 proportionally increased with the number of cycles under thermal shock test conditions. The electrical resistance of ICA 2 also increased proportionally during the first 600 cycles, but increased rapidly thereafter. The rapid temperature changes of the thermal shock test causes shrinkage and expansion of substrates, eventually leading to an increase in electrical resistance.<sup>11)</sup> Interestingly, when compared with the conventional ICAs, the SCA assembly showed much more stability in terms of electrical resistance when subjected to this test.

Figure 4 shows the electrical resistance changes of conventional ICAs and SCA assemblies during the high

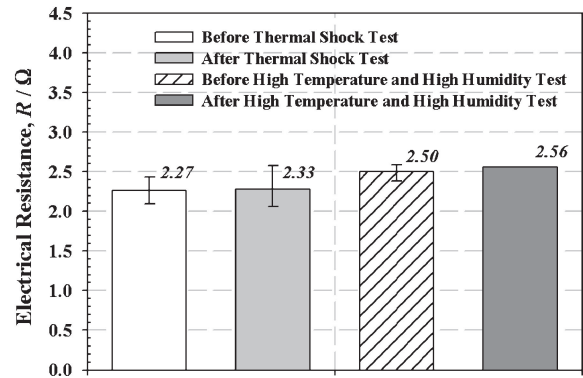


Fig. 5 Electrical resistance shift of SCA assemblies before and after reliability test.

temperature and high humidity test. The conventional ICAs, ICA 1 and ICA 2, showed extreme changes in electrical resistance, while the changes in ICA 3 were proportional. Electrical resistance increased as test time increased in the high humidity condition, likely caused by moisture absorption by the adhesive and resulting in surface oxidation of particles and metallization, adhesion degradation, and hygroscopic expansion.<sup>12,13)</sup> Again, the SCA assembly showed excellent electrical properties, even though the initial electrical resistance increased slightly. It has been proposed that the increase in electrical resistance between ICA and Cu-finished board during temperature and humidity aging is due to galvanic corrosion of the non-noble metal surfaces.<sup>14)</sup>

The electrical resistance and mechanical pull strength of SCA assemblies before and after reliability tests are shown in the Fig. 5 and Fig. 6, respectively. As shown in Fig. 5, the electrical resistances before and after the thermal shock test were 2.27 and 2.33 Ω (about a 2.6% increase), respectively. The electrical resistances before and after the high temperature and high humidity test were 2.50 and 2.56 Ω (about a 2.4% increase), respectively. The results of our reliability tests strongly suggest that the SCA assembly has more stable electrical conductance. On the other hand, as shown in Fig. 6, pull strengths after the thermal shock and high temperature and high humidity tests were 17.84 and 14.16 N, respectively. Pull strength was decreased about 8.7% after the thermal

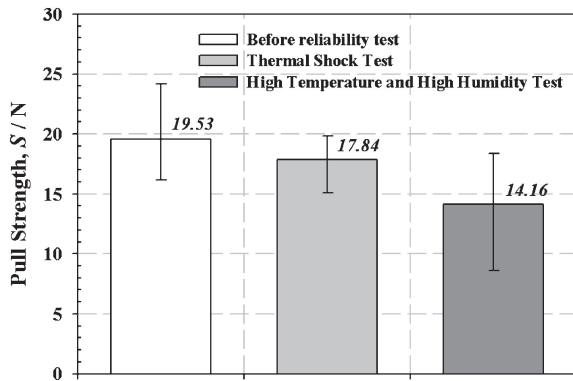


Fig. 6 Mechanical pull strength shift of SCA assemblies before and after reliability test.

shock test and 27.5% after the high temperature and high humidity tests when compared to the initial pull strength of 19.53 N. The change in mechanical pull strength was caused by a decrease in adhesion caused by moisture absorption into the polymer matrix and the increase in brittleness on the bonding interface was caused by excessive expansion of the IMCs.

### 3.2 Microstructure and failure analysis

To investigate the interface microstructure and the mode of fracture of SCA joints, cross-sectional studies and failure analysis were conducted for each reliability test.

Cross-sectional FE-SEM images of SCA joints before and after the reliability tests are shown in the Figs. 7–9. The QFP

joint using the SCA was composed of a metallurgical conduction path of molten LMPA filler and a cured polymer region (outside of the conduction path). The cross-sectional images of SCA joints before reliability testing are shown in Fig. 7. As shown in the figure, the most of LMPA fillers were coalesced and wet on the upper and lower metallization. It can be seen that the wetted coalesced LMPA formed a good fillet shape at the heel and toe region of QFP lead and the stable metallurgical interconnection could be achieved by the LMPA fillers. The spherical LMPA fillers remained outside the interconnection region. Since the remaining LMPA fillers were covered with the polymer matrix, the QFP assembly maintained its insulation properties between adjacent leads. Previous study has shown that the reduction capability of polymer matrix is indispensable for the stable metallurgical interconnection, and must have a sufficient reduction capability against the used LMPA material and metallization.<sup>15)</sup>

At the interface between the Sn-plated Cu lead and the LMPA filler, scallop-type  $\text{Cu}_6\text{Sn}_5$  ( $\eta$ -phase) IMC with a thickness of 1–3  $\mu\text{m}$  was formed, which was caused by the interfacial reaction of the Cu lead and liquid Sn. Residual Bi from the LMPA filler was concentrated at the IMC and solder interface. In addition, a scallop-type  $\text{Cu}_6\text{Sn}_5$  ( $\eta$ -phase) IMC with a thickness of about 1–2  $\mu\text{m}$  was formed at the interface of the Cu metallization of the PCB and the LMPA filler. A small amount of  $\text{Cu}_3\text{Sn}$  ( $\epsilon$ -phase) was measured between the  $\text{Cu}_6\text{Sn}_5$  IMC layer and the Cu metallization by EDS analysis. However, as shown in Figs. 8–9, the total IMC layers after reliability testing grew, and the scallop-type IMC transformed into a layer-type IMC. The IMC layer consisted of two

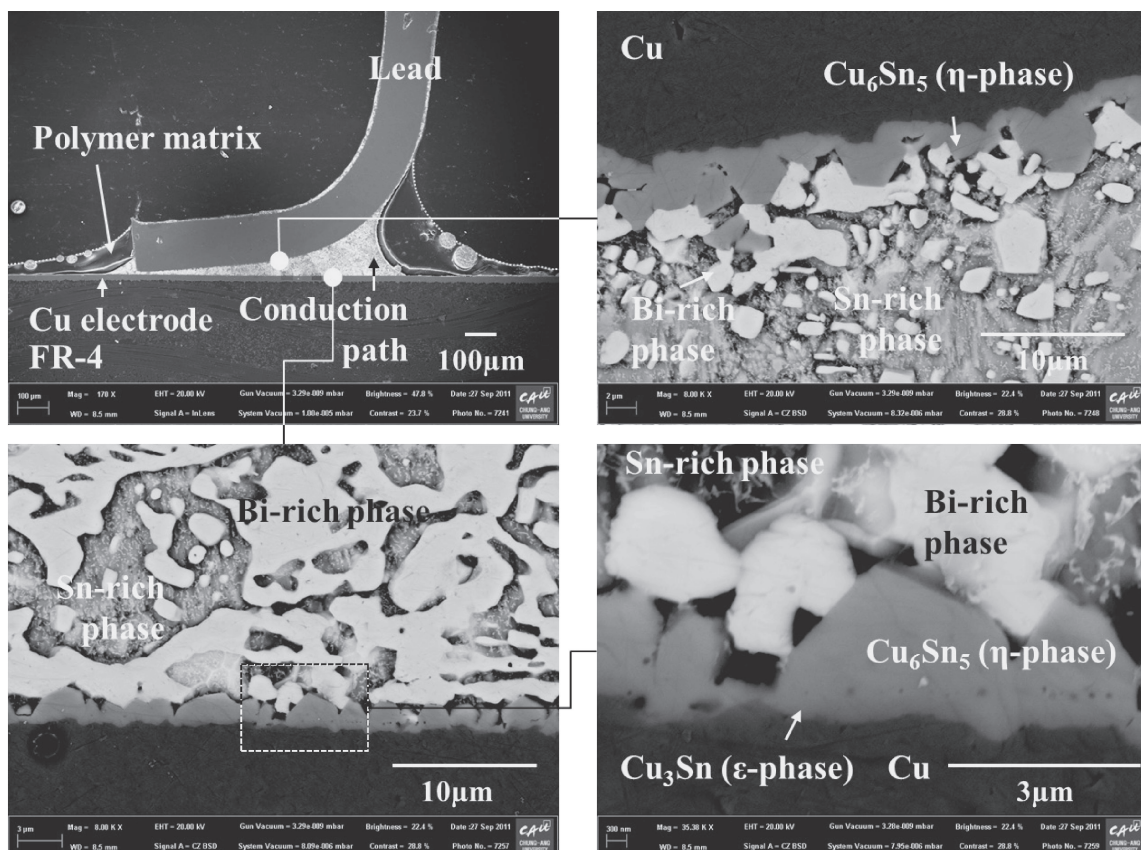


Fig. 7 The interfacial microstructure of the QFP joint using SCA before reliability test.

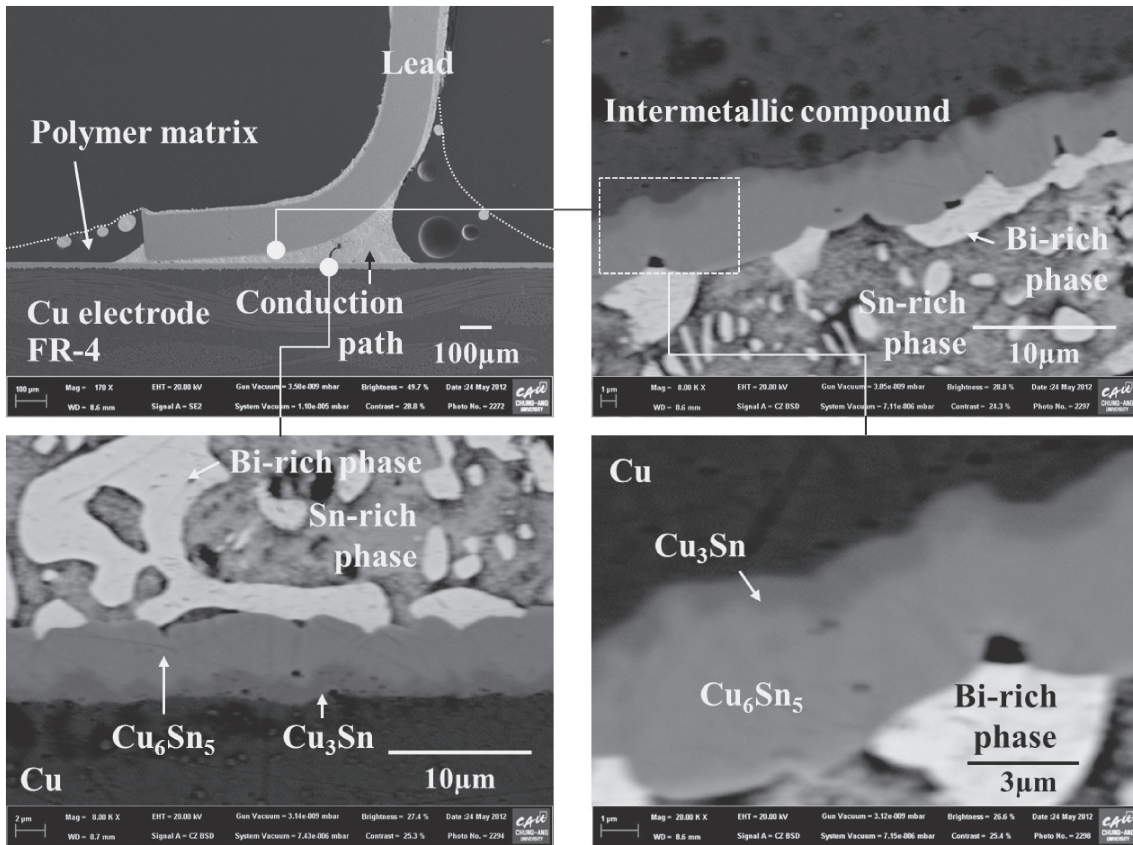


Fig. 8 The interfacial microstructure of the QFP joint using SCA after thermal shock test.

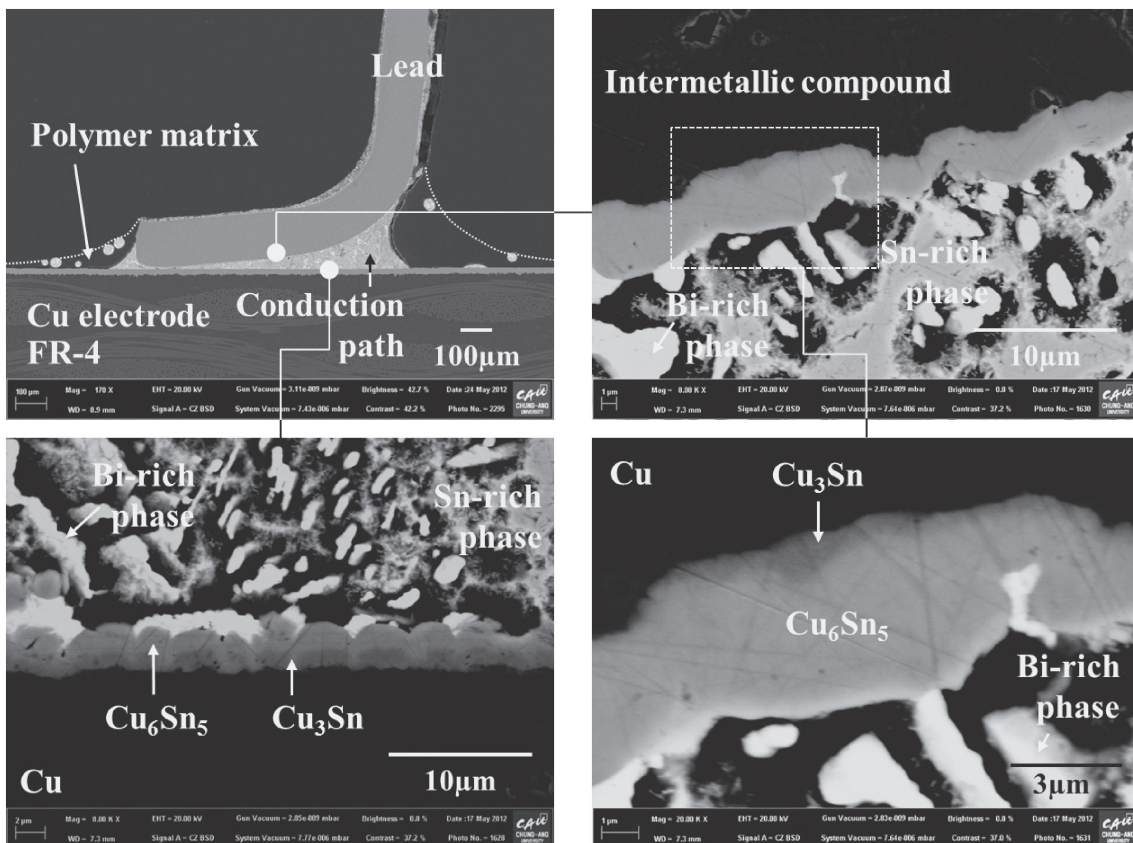


Fig. 9 The interfacial microstructure of the QFP joint using SCA after high temperature and high humidity test.

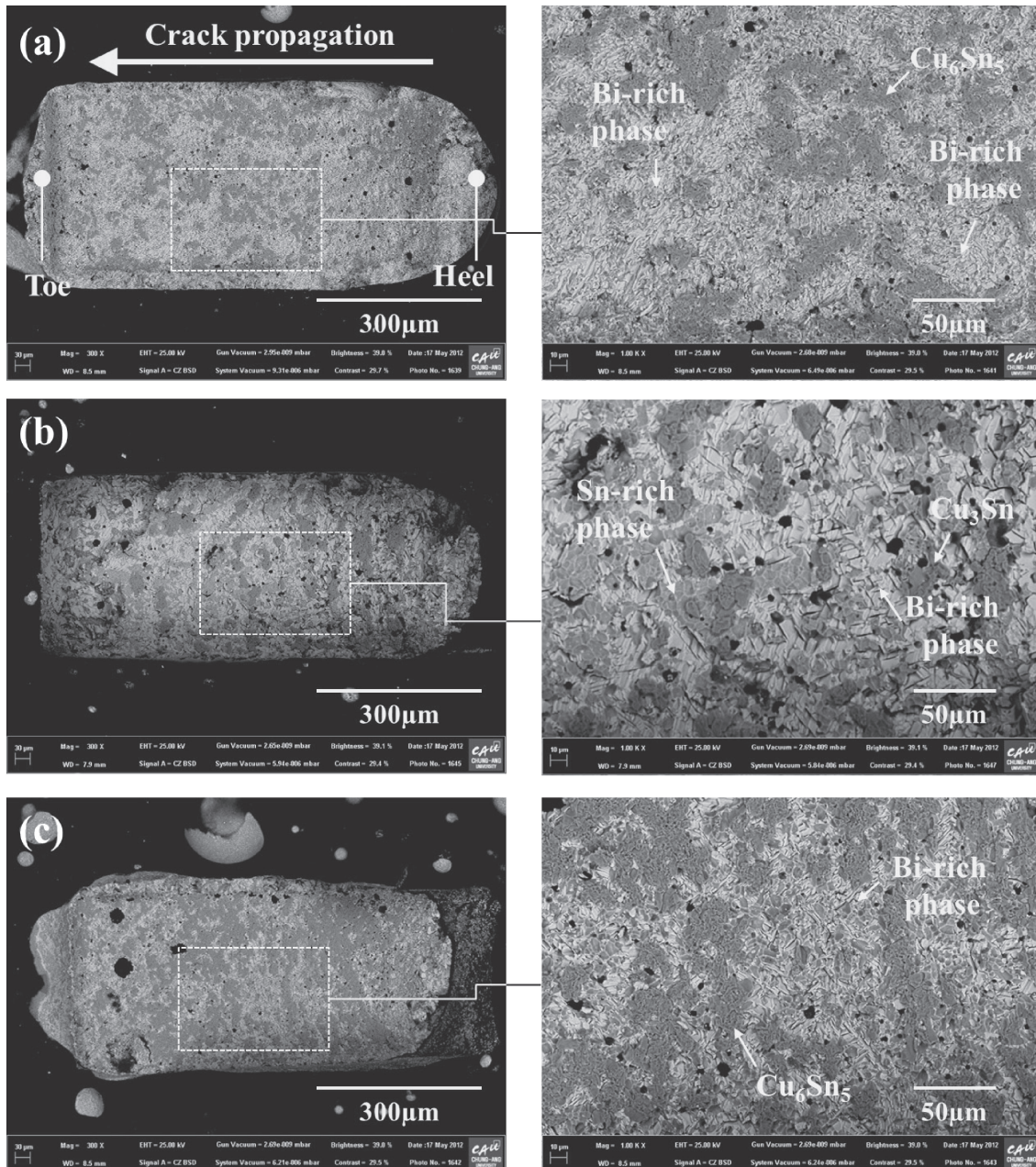


Fig. 10 Morphologies of the fracture surface of the SCA joints. (a) Before reliability testing, (b) after the thermal shock test, and (c) after the high temperature and high humidity test.

clearly separated layers and the compositions of the interfacial structure were formed with  $\text{Cu}_6\text{Sn}_5$  and  $\text{Cu}_3\text{Sn}$  IMC. In the IMC growth process, Cu from the metallization diffused to the solder/ $\text{Cu}_6\text{Sn}_5$  interface by volume or grain boundary diffusion and reacted with Sn to form  $\text{Cu}_6\text{Sn}_5$  IMC (1) at the  $\text{Cu}_6\text{Sn}_5/\text{Cu}$  interface. In addition,  $\text{Cu}_3\text{Sn}$  IMC was formed by the reaction between  $\text{Cu}_6\text{Sn}_5$  and Cu metallization (2).<sup>16,17)</sup>



In response to thermal shock, the total thickness of the IMC layer increased to 4–6  $\mu\text{m}$  ( $\text{Cu}_3\text{Sn}$  IMC: 1  $\mu\text{m}$ ) at the Cu lead/LMPA filler interface and to 5–6  $\mu\text{m}$  ( $\text{Cu}_3\text{Sn}$  IMC: 1–2  $\mu\text{m}$ ) at the LMPA filler/Cu metallization interface. In high temperature and high humidity testing, the total IMC

thickness was approximately 4  $\mu\text{m}$  ( $\text{Cu}_3\text{Sn}$  IMC: 0.5–1  $\mu\text{m}$ ) at the lead/LMPA filler interface and 2–3  $\mu\text{m}$  ( $\text{Cu}_3\text{Sn}$  IMC: 0.5–1  $\mu\text{m}$ ) at the interface of LMPA filler/Cu metallization.

Brittleness caused by excessive intermetallic accumulation degrades interfacial integrity and induces a mismatch in physical properties such as the coefficient of thermal expansion (CTE) and the elastic modulus. As a result, the thermal fatigue life, tensile strength, and fracture toughness of solder joints are compromised by increases in the Cu–Sn IMC layer.<sup>18,19)</sup> We therefore expected that the pull strengths after the thermal shock and high temperature and high humidity tests would be decreased secondary to increases in the Cu–Sn IMC layer. The fracture surface morphologies of SCA joints before and after each reliability test are shown in Fig. 10. Two images of each specimen are presented: one of the entire fracture surface at a relatively low magnification

and one at a higher magnification. As shown in the results, at every SCA joint the initiating breakage point began at the top of the heel side and propagated toward the toe side along the solder/IMC interface. Prior to reliability testing (Fig. 10(a)), the crack propagated through the solder/Cu<sub>6</sub>Sn<sub>5</sub> interface and the fracture surface was composed of two regions: perfect Cu<sub>6</sub>Sn<sub>5</sub> grains and cracked Bi-rich solder. This indicated that most fractures were fundamentally propagated within the Bi-rich phase close to the IMC layer.<sup>20)</sup> In addition, the fracture surface showing a semi-brittle fracture mode contained quasi-cleavage fractures mixed with cleavage and ductile tear bands.

On the other hand, as shown in the Fig. 10(b), the fracture surface after thermal shock had a dimpled surface of Sn-rich solder, a cleaved surface of Bi-rich solder and Cu<sub>3</sub>Sn grains. Under the thermal shock test, the size of the Bi-rich phase increased at the solder side of the solder/Cu<sub>6</sub>Sn<sub>5</sub> interface caused by the consumption of Sn from bulk solder to Cu<sub>6</sub>Sn<sub>5</sub> IMC. The cleavage fracture occurred along the Bi-rich phase boundary. The mechanical strength of joints degrades through these phenomena.<sup>21)</sup> The crack propagated along the Sn-rich solder/IMC interface and through the brittle Bi-rich phase.<sup>22)</sup>

The fracture surface after the high temperature and high humidity test (Fig. 10(c)) showed a very similar fracture mode and chemical composition compared with before reliability test. Though interfacial IMC was increased (see Fig. 9), the crack still propagated through the solder/Cu<sub>6</sub>Sn<sub>5</sub> interface. The fracture surface was composed of Cu<sub>6</sub>Sn<sub>5</sub> grains and cracked Bi-rich solder. In addition, the fracture was semi-brittle and contained quasi-cleavage fractures. The Bi segregation at the Cu/Cu<sub>3</sub>Sn interface was not investigated here. In addition, increased void formations were observed on the fracture surface after reliability testing (Fig. 10(b), (c)). The Sn–Bi eutectic solder had a serious voiding problem due to its low melting point. As the presence of voids reduces the effective joint area, the mechanical strength would be decreased.<sup>23)</sup>

#### 4. Conclusion

In this study we investigated the reliability properties of SCA with LMPA filler particles. By thermal shock and high temperature and high humidity testing, the SCA assemblies showed good electrical stability, which resulted from the formation of stable metallurgical interconnections. The mechanical strength of the assemblies was decreased about 8.7% after thermal shock testing and 27.5% after high temperature and high humidity testing, compared with initial

pull strength before reliability testing due to the increase in the brittleness of the bonding interface caused by excessive growth of the IMCs and the increase in void formation in the SCA joints. In summary, the SCA had excellent electrical and mechanical reliability properties when compared with conventional ICAs.

#### Acknowledgements

This research was supported by the Chung-Ang University Research Grants in 2009.

#### REFERENCES

- 1) F. Tan and X. Qiao: *Int. J. Adhes. Adhes.* **26** (2006) 406–413.
- 2) M. J. Yim, Y. Li, K. S. Moon, K. W. Paik and C. P. Wong: *J. Adhes. Sci. Technol.* **22** (2008) 1593–1630.
- 3) A. Seppealea and E. Ristolainen: *Microelectron. Reliab.* **44** (2004) 639–648.
- 4) M. Zwolinski, J. Hickman, H. Rubin, Y. Zaks, S. McCarthy, T. Hanlon, P. Arrowsmith, A. Chaudhuri, R. Harmansen, S. Lau and D. Napp: *IEEE Trans. Compon. Packag. Manuf. Tech. C* **19** (1996) 241–250.
- 5) K. S. Moon, J. Wu and C. P. Wong: *IEEE Trans. Compon. Packag. Tech.* **26** (2003) 375–381.
- 6) S. K. Kang and S. Purushothaman: *J. Electron. Mater.* **28** (1999) 1314–1318.
- 7) B. S. Yim, J. M. Kim, S. H. Jeon, S. H. Lee, J. h. Kim, J. G. Han, Y. S. Eom and Y. E. Shin: *Mater. Trans.* **50** (2009) 1684–1689.
- 8) B. S. Yim, J. M. Kim, S. H. Jeon, S. H. Lee, J. H. Kim, J. G. Han and M. H. Cho: *Mater. Trans.* **50** (2009) 2649–2655.
- 9) K. W. Moon, W. J. Boettinger, U. R. Kattner, C. A. Handwerker and D. J. Lee: *J. Electron. Mater.* **30** (2001) 45–52.
- 10) B. S. Yim and J. M. Kim: *Mater. Trans.* **51** (2010) 2329–2331.
- 11) S. K. Park, J. I. Han, W. K. Kim and M. G. Kwan: *Jpn. J. Appl. Phys.* **40** (2001) 412–418.
- 12) J. Y. Kim, S. Kwon and D. W. Ihm: *J. Mater. Process. Technol.* **152** (2004) 357–362.
- 13) J. H. Zhang, Y. C. Chang, M. O. Alam and S. Fu: *Microelectron. Reliab.* **43** (2003) 1303–1310.
- 14) D. Lu, Q. K. Tong and C. P. Wong: *IEEE Trans. Electron. Pack. Manuf.* **22** (1999) 228–232.
- 15) B. S. Yim, Y. Kwon, S. H. Oh, J. Kim, Y. E. Shin, S. H. Lee and J. M. Kim: *Microelectron. Reliab.* **52** (2012) 1165–1173.
- 16) C. Z. Liu and W. Zhang: *J. Mater. Sci.* **44** (2009) 149–153.
- 17) T. Y. Kang, Y. Y. Xiu, C. Z. Liu, L. Hui, J. J. Wang and W. P. Tong: *J. Alloy. Compd.* **509** (2011) 1785–1789.
- 18) J. W. Yoon and S. B. Jung: *J. Alloy. Compd.* **359** (2003) 202–208.
- 19) P. L. Tu, Y. C. Chan and J. K. L. Lai: *IEEE Trans. Compon. Packag. Manuf. Technol. B* **20** (1997) 87–93.
- 20) Q. S. Zhu, Z. F. Zhang and Z. G. Wang: *J. Mater. Res.* **23** (2008) 78–82.
- 21) P. J. Shang, Z. Q. Liu, D. X. Li and J. K. Shang: *J. Electron. Mater.* **38** (2009) 2579–2584.
- 22) C. H. Reader, L. E. Felton, V. A. Tanzi and D. B. Knorr: *J. Electron. Mater.* **23** (1994) 611–617.
- 23) N. M. Poon, C. M. L. Wu, J. K. L. Lai and Y. C. Chan: *IEEE Trans. Adv. Packag.* **23** (2000) 708–714.